Calibration of CRL all-sky imagers using an integrating sphere

Masa-yuki Yamamoto[1], Minoru Kubota[1], Shu Takeshita[2],
Mamoru Ishii[1], Yasuhiro Murayama[1] and Masaki Ejiri[2]

[1]*Communications Research Laboratory, 4-2-1 Nukui-kitamachi, Koganei-shi, Tokyo 184-8795*
[2]*National Institute of Polar Research, Kaga 1-chome, Itabashi-ku, Tokyo 173-8515*

Abstract: As part of an international collaboration with the Geophysical Institute of the University of Alaska, we have developed two all-sky imagers (CRL-ASIs). A sensitivity calibration of the CRL-ASIs was performed using an integrating sphere belonging to the National Institute of Polar Research (NIPR). The two-dimensional sensitivities of the CRL-ASIs produced symmetrical distributions. Using this sensitivity data, we converted airglow/aurora images into two-dimensional distributions of absolute intensity. The sensitivity of the CRL-ASIs was measured for 13 wavelengths between 427.8 nm and 866.5 nm, and the relationship between the sensitivity and the wavelength was investigated for both imagers. The peak sensitivity occurred at about 550 nm.

1. Introduction

Multiple wavelength observations of aurora/airglow emissions obtained with an all-sky imager, consisting of a bare cooled CCD camera and interference filters with a narrow band passage, have been frequently used as a practical method of producing sensitive images during the past decade (*e.g.*, Taylor *et al.*, 1995; Ejiri *et al.*, 1997; Kubota *et al.*, 2000).

The Joint Program of the Middle and Upper Atmosphere Observation (Alaska Project) was begun in 1995 by the Communications Research Laboratory (CRL) and the Geophysical Institute, University of Alaska Fairbanks, USA. As part of this project, we developed two all-sky imagers (CRL-ASIs). Continuous observation of aurora/airglow emissions by the CRL-ASIs began in October 2000, at the Poker Flat Research Range, Alaska (Latitude: 65.12°N, Longitude: 147.43°E, and Geomagnetic latitude: 65.60°N). Since the two CRL-ASIs are located at the same observation site, we can simultaneously observe auroral images of two independent wavelengths with no time separation. Using this advantage, we plan to estimate the two-dimensional energy deposition rate of precipitating auroral particles. The energy flux and the characteristic energy of the precipitating particles can be estimated using the absolute intensity of 427.8 nm emissions and the ratio of auroral emission intensities of two different wavelengths, respectively (Rees and Luckey, 1974; Rees *et al.*, 1988; Ono, 1993). For this estimation, the absolute intensity distribution of the auroral emissions must be obtained. Therefore, we first

calibrated the sensitivities of the CRL-ASIs using an integrating sphere.

Absolute two-dimensional calibration of an all-sky imaging system can be obtained using an integrating sphere, which has a uniform light source that fills a 2π-steradian field of view. The uniformity of the radiance in the 1.9-m integrating sphere, which belongs to the National Institute of Polar Research (NIPR), is better than $\pm 5\%$ for a 2π field of view (Okano *et al.*, 1998). Shiokawa *et al.* (2000) reported calibration results for three imagers developed by the Solar-Terrestrial Environment Laboratory of Nagoya University. In their report, they mentioned that filters with highly flattened image-quality surfaces may cause serious Newton's Ring patterns on the final images. In our study, we measured the two-dimensional sensitivities of the CRL-ASIs at 13 wavelengths and investigated the relationship between sensitivity and wavelength.

2. Instrumentation and calibration method

Each CRL-ASI consists of two sections: an optical section, with a wide-field lens (Nikon, 6 mm, F1.4, FOV=180°), interference filters, and tele-centric lens system; and a detector section, with a bare cooled CCD camera (Pixel Vision, 512×512 pixels, back-illuminated). Both CRL-ASIs have the same configuration. Five filters can be installed in the filter turret of each CRL-ASI. Figure 1 shows one of the CRL-ASIs being calibrated with the integrating sphere (Optronic Laboratories Inc., OL462-80A). The integrating sphere has an internal diameter of 1.9 m. Its specially coated inner surface was carefully manufactured to achieve uniform reflection. The lamp luminosity of the integrating sphere was constantly monitored during the experiment. The transmission profiles
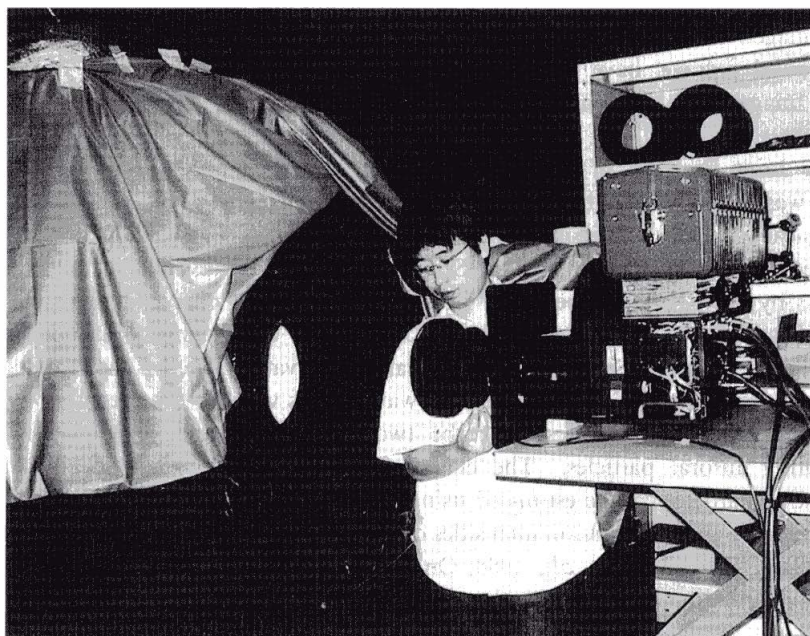

Fig. 1. CRL-ASI being calibrated with the 1.9-m integrating sphere from NIPR.

of the interference filters were measured using the auto spectro-photometer at NIPR (Hitachi. Ltd.. U-3300).

During the aurora/airglow emission measurements using the CRL-ASI, the observed value $C_{AG}[Count]$ was given by the following equation (*e.g.*, Shiokawa *et al.*, 2000; Kubota *et al.*, 2001):

$$\langle C_{AG} \rangle = a \cdot E_{AG} \int_0^{\infty} \langle T_{opt}(\lambda) \rangle \cdot \langle S_{CCD}(\lambda) \rangle \cdot \{\langle I_{AG}(\lambda) \rangle + \langle I_{BG}(\lambda) \rangle\} \cdot T_{AG}(\lambda) d\lambda, \quad (1)$$

where $a[Count/Rayleigh/s]$ is a constant, $E_{AG}[s]$ is the exposure time, $T_{opt}[\%]$ is the transmission of the optical section without the interference filter, $S_{CCD}[\%]$ is the sensitivity of the CCD camera (determined by multiplying the quantum efficiency of the CCD [*electrons/photon*] and the conversion efficiency [*Count/electron*]), $I_{AG}[Rayleigh]$ is the absolute intensity of the aurora/airglow emission, $I_{BG}[Rayleigh/nm]$ is the absolute intensity of the background continuum, and $T_{AG}[\%]$ is the transmission of the interference filter. The values enclosed by $< >$ indicate the two-dimensional variables at the focal plane. In general, $T_{AG}[\lambda]$ becomes a two-dimensional variable because the filter transmission peak is shifted towards shorter wavelength at the edge of an image as a result of oblique incoming light. In eq. (1), however, $T_{AG}[\lambda]$ is described as a fixed value at the center of the image. This point will be discussed in grater detail in the Discussion section. From eq. (1), the following equation can be derived:

$$\langle C_{AG} \rangle = a \cdot E_{AG} \int_0^{\infty} \langle T_{opt}(\lambda) \rangle \cdot \langle S_{CCD}(\lambda) \rangle \cdot \{\langle I_{AG}(\lambda) \rangle \delta(\lambda - \lambda_{AG}) + \langle I_{BG}(\lambda) \rangle\} \cdot T_{AG}(\lambda) d\lambda$$

$$= a \cdot \langle T_{opt}(\lambda_{AG}) \rangle \cdot \langle S_{CCD}(\lambda_{AG}) \rangle \cdot E_{AG} \{\langle I_{AG}(\lambda_{AG}) \rangle \cdot T_{AG}(\lambda_{AG})$$

$$+ \langle I_{BG}(\lambda_{AG}) \rangle \cdot \int_0^{\infty} T_{AG}(\lambda) d\lambda\}, \quad (2)$$

where the variation of T_{opt} and S_{CCD} with different wavelengths within the filter pass band is assumed to be negligible.

To obtain the absolute intensity I_{AG}, simultaneous measurement of the background intensity I_{BG} is needed to enable the background to be subtracted. $T_{AG}(\lambda_{AG})$, $\int_0^{\infty} T_{AG}(\lambda) d\lambda$, and $a \cdot \langle T_{opt}(\lambda_{AG}) \rangle \cdot \langle S_{CCD}(\lambda_{AG}) \rangle$ are required for the calibration: $T_{AG}(\lambda_{AG})$ and $\int_0^{\infty} T_{AG}(\lambda) d\lambda$ can be obtained by measuring the transmission profiles of the interference filters, while $a \cdot \langle T_{opt}(\lambda_{AG}) \rangle \cdot \langle S_{CCD}(\lambda_{AG}) \rangle$ [$Count/Rayleigh/s$] can be derived using the integrating sphere in the manner described below.

The integrating-sphere image $\langle C_{Integ} \rangle [Count]$ obtained by the CRL-ASIs can be described as

$$\langle C_{Integ} \rangle = a \cdot \langle T_{opt}(\lambda_{AG}) \rangle \cdot \langle S_{CCD}(\lambda_{AG}) \rangle \cdot E_{Integ} \cdot \int_0^{\infty} \langle I_{Integ}(\lambda) \rangle T_{AG}(\lambda) d\lambda, \quad (3)$$

where $E_{Integ}[s]$ is the exposure time and $\langle I_{Integ}(\lambda) \rangle [Rayleigh/nm]$ is the luminosity of the integrating sphere. Since $\langle I_{Integ}(\lambda) \rangle$ has been carefully determined beforehand, $a \cdot \langle T_{opt}(\lambda_{AG}) \rangle \cdot \langle S_{CCD}(\lambda_{AG}) \rangle$ can be calculated using eq. (3).

3.   Results

Figure 2a shows the two-dimensional distribution of CRL-ASI sensitivity at a wavelength of 557.7 nm.   The sensitivity drops symmetrically from the center toward the edge of the image due to vignetting.   Figure 2b shows two cross sections of the sensitivity along the horizontal and vertical lines that cross at the center of Fig. 2a.   Both cross sections are nearly identical, suggesting that the alignment of the CRL-ASI optical system was well adjusted and that the CRL-ASI can be used for all-sky imaging with excellent results.   The sensitivity values along the vertical cross line are slightly higher than the
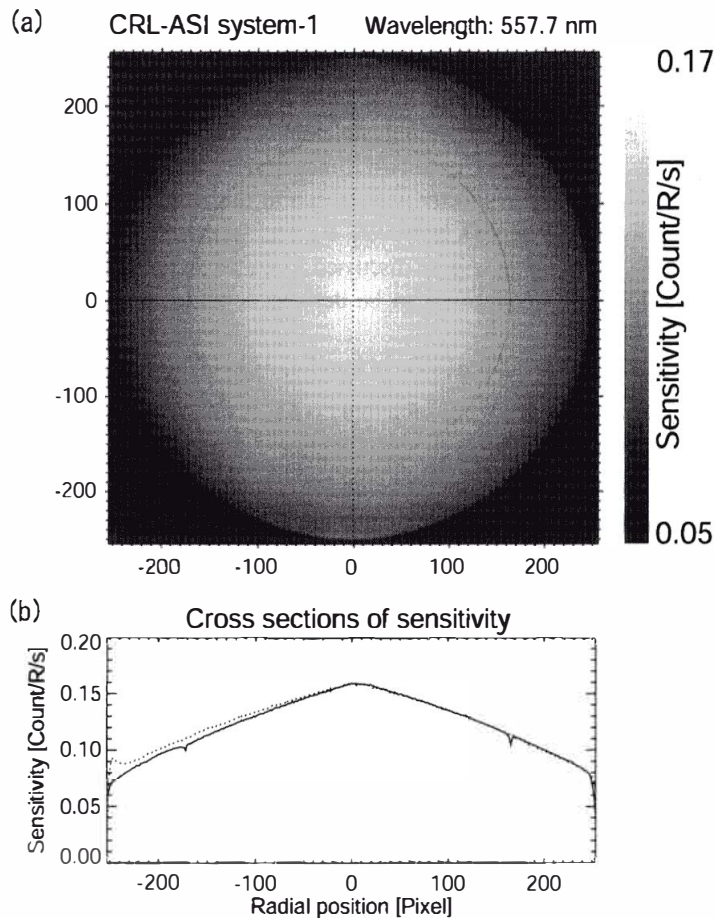

Fig. 2.   *(a) Two-dimensional distribution of the CRL-ASI sensitivity (at 557.7 nm).   The circle seen in the image represents the joint where the two hemispheres that form the integrating sphere meet.   (b) Cross sections of the sensitivity data shown in (a).   The solid and broken lines represent the cross sections of the sensitivity data along the horizontal and vertical lines that cross at the center of the image in (a), respectively. The joint where the hemispheres meet appears as a dip at about ±170 pixels.   The small "bump" seen at −250 pixels in the vertical cross section represents a localized nonuniformity of the inner surface of the integrating sphere.*
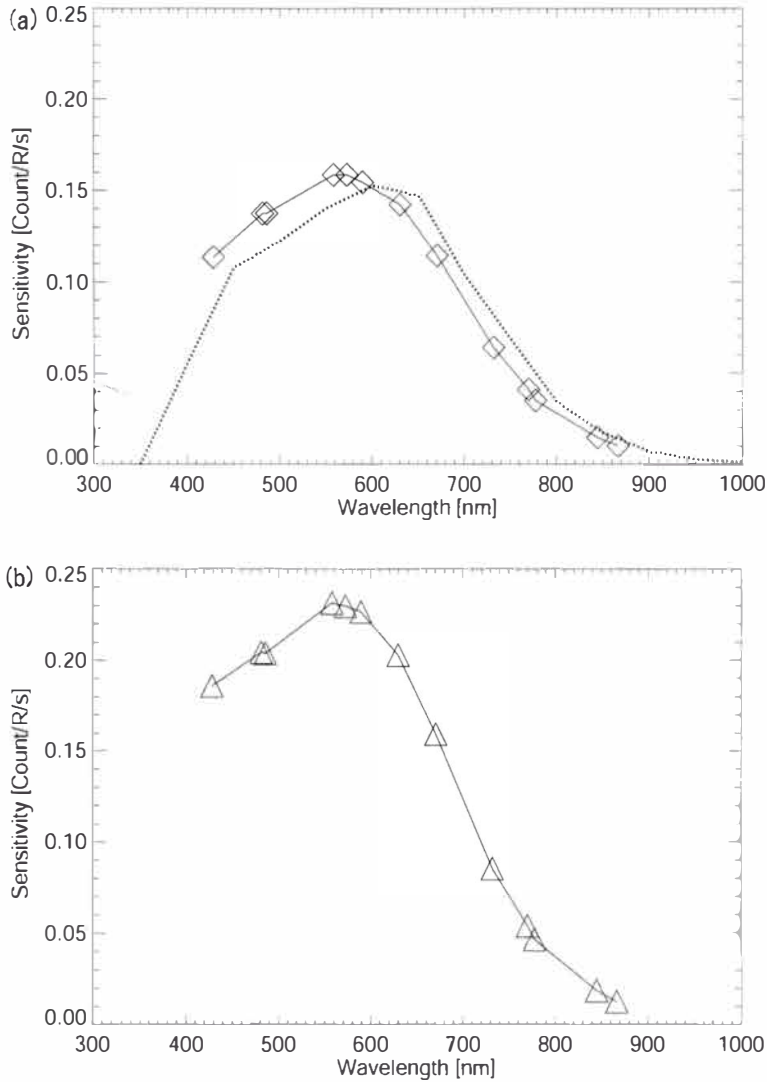
Fig. 3. (a) Relationship between sensitivity and wavelength for CRL-ASI system-1. The dotted line shows the reference sensitivity derived from the transmission rate of the optical system and the quantum efficiency of the CCD device, based on data provided by the manufacturer. (b) Relationship between sensitivity and wavelength for CRL-ASI system-2.

values along the horizontal one between -240 and -20 pixels, as seen in Fig. 2b, and a "bump" occurs on the edge of the image at -250 pixels. The higher value seen at the bottom edge of the image seems to be caused by a localized nonuniformity of the inner surface radiance of the integrating sphere. However, the difference between the two cross sections is less than 7% if the "bump" is excluded. Since the integrating sphere consists of two hemispheres, the mating joint of the two hemispheres is seen as small dips at about

Table 1.   *Listing of filter specifications. All filters were made by Andover Co. with options of 'type 3', 'block to FIR', and 'non image quality'.*

Center wavelength (nm)	FWHM (nm)	T_{AG} (λ_{AG})(%)	Objective emission
427.9	2.8	41.0	N_2^+ 1NG(0.1)
481.25	1.7	45.1	Background for Hβ
485.75	1.7	46.8	Hβ
557.6	2.0	52.8	OI
572.2	2.0	61.6	background
589.05	2.3	59.7	Na
630.0	2.2	68.6	OI
670.65	2.9	53.9	N_2
732.05	2.1	54.8	O^+
770.0	3.0	59.6	K
777.6	2.8	62.5	OI
844.7	2.6	54.5	OI
866.5	9.4	82.8	O_2(0.1)

± 170 pixels in the cross sections, which is also seen as a circle on the image.   However, this does not seriously affect the results of the observation because the dips can be removed using a smoothing process over a region of 10×10 pixels.

Figure 3a shows the variations in sensitivity between 427.8 nm and 866.5 nm for CRL-ASI system-1, and Fig. 3b shows the same data for CRL-ASI system-2.   Each sensitivity value indicates the averaged value for 10×10 pixels at the center of the image (zenith direction).   The maximum sensitivity value was observed at about 557.7 nm.   A list of the 13 interference filters used in the present investigation is shown in Table 1.   The sensitivity of system-2 was somewhat higher than that of system-1, though the two CRL-ASIs were manufactured using the same design.   However, the sensitivity distributions of the two CRL-ASIs indicate that their features are similar.

4. Discussions

In eq. (1), $T_{AG}(\lambda)$ can be expressed as a fixed value at the image center if λ_{AG} is situated on the shorter wavelength side of the flat portion of the filter transmission.   Most of the Andover Type 3 filters listed in Table 1 satisfy this condition.   For the OI (557.7 nm) and Hβ (485.9 nm) emissions, however, the corresponding filters fail to meet this condition.   Nevertheless, the absolute intensity of these emissions can be correctly calibrated at almost any portion of the image except for at the edge.

As is well known, filter transmission shifts with temperature.   This may cause the absolute calibration factor to vary when the imagers are used at a different temperature from that in the integrating sphere.   In the present case, however, the shift was negligible because the imagers were placed in an air-conditioned room at room temperature in the

observatory building at Poker Flat.

By comparing Figs. 3a and 3b, the sensitivity of CRL-ASI system-2 was found to be about 1.4 times higher than that of CRL-ASI system-1 at each wavelength. This difference seems to be caused by a difference in the gain setting of the conversion efficiency from the number of electrons to the output count rate. In general, the quality of an image can be evaluated by the S/N ratio. The difference in sensitivity between the two CRL-ASIs is not considered to affect the S/N ratio of the image for the following reason. Since the noise of the imager system consists of thermal noise, readout noise, and statistical random noise, the S/N ratio of the image data is determined before the conversion process. Namely, the signal and noise are amplified together at the same rate in the conversion process, so the S/N ratio remains constant and is independent of the conversion process' gain setting.

Using the sensitivity data, the optimum exposure time for the aurora/airglow emissions can be determined for each wavelength. The exposure time is determined by considering the time resolution and S/N ratio. For the present CRL-ASI set-up, the dark noise is about 0.5 $[Counts/pixel/s]$ and the readout noise is about 12 $[Counts, rms]$. The statistical random noise associated with the quantum effect in the CCD is equal to the square root of the signal count rate. In the case of a typical green aurora with an intensity of 3 $[k\ Rayleigh]$ when observed at a wavelength of 557.7 nm, a high-quality image with an S/N ratio of 35 can be obtained using a 3-second exposure. For an aurora with an intensity of 500 $[Rayleigh]$ at a wavelength of 844.6 nm, an image with an S/N ratio of 8 can be obtained using a 45-second exposure.

5. Summary

The sensitivity of two CRL-ASIs was calibrated using an integrating sphere. The two-dimensional sensitivities of the CRL-ASIs exhibited symmetrical distributions. Calibration data were obtained for 13 wavelengths between 427.8 nm and 866.5 nm, and the relationship between sensitivity and wavelength was analyzed for each CRL-ASI. The absolute intensity of the aurora/airglow emission can be calculated from the CRL-ASI observations using the results of the accurate sensitivity calibration. The two-dimensional absolute intensity of the aurora emission is useful for estimating the energy flux and characteristic energy of the precipitating auroral particles.

Using the filters listed in Table 1, observations of aurora/airglow emissions at altitudes ranging from the mesopause region to the F-region can be used to quantitatively investigate atmospheric and ionospheric dynamics in this region.

Acknowledgments

References

Ejiri, M., Okano, S., Okada, M., Taguchi, M. and Takeshita, S. (1997): All sky imager observation of aurora and airglow at South Pole: System design and the initial test results (extended abstract). Proc. NIPR Symp. Upper Atmos. Phys., **11**, 159–162.

Kubota, M., Shiokawa, K., Ejiri, M.K., Otsuka, Y., Ogawa, T., Sakanoi, T., Fukunishi, H., Yamamoto, M., Fukao, S. and Saito, A. (2000): Traveling ionospheric disturbances observed in the OI 630-nm nightglow images over Japan by using a multipoint imager network during the FRONT campaign. Geophys. Res. Lett., **27**, 4037–4040.

Kubota, M., Fukunishi, H. and Okano, S. (2001): Characteristics of medium- and large-scale TIDs over Japan derived from OI 630-nm nightglow observation. Earth Planets Space, **53**, 741–751.

Okano, S., Takeshita, S. and Taguchi, M. (1998): Absolute calibration system at NIPR for aurora/airglow measurements using a 1.9-m integration sphere. Proc. 24th Annual European meeting on Atmospheric Studies by Optical method, 30.

Ono, T. (1993): Derivation of energy parameters of precipitating auroral electrons by using the intensity ratios of auroral emissions. J. Geomagn. Geoelectr., **45**, 455–472.

Rees, M.H. and Luckey, D. (1974): Auroral electron energy derived from ratio of spectroscopic emissions 1. Model computations. J. Geophys. Res., **79**, 5181–5186.

Rees, M.H., Lummerzheim, D., Roble, R.G., Winningham, J.D., Craven, J.D. and Frank L.A. (1988): Auroral energy deposition rate, characteristic electron energy, and ionospheric parameters derived from Dynamics Explorer 1 images. J. Geophys. Res., **93**, 12841–12860.

Shiokawa, K., Katoh, Y., Satoh, M., Ejiri, M.K. and Ogawa, T. (2000): Integrating-sphere calibration of all-sky cameras for nightglow measurements. Adv. Space Res., **26**, 1025–1028.

Taylor, M.J., Bishop, M.B. and Taylor, V. (1995): All-sky measurements of short period waves imaged in the OI(557.7 nm), Na(589.2 nm) and near infrared OH and $O_2(0,1)$ nightglow emissions during the ALOHA-93 campaign. Geophys. Res. Lett., **22**, 2833–2836.